Materials Chemistry

PAPER

Luminescence tuning of MOFs *via* ligand to metal and metal to metal energy transfer by co-doping of $^2_\infty$[Gd$_2$Cl$_6$(bipy)$_3$]·2bipy with europium and terbium†

P. R. Matthes,[a] C. J. Höller,[a] M. Mai,[b] J. Heck,[b] S. J. Sedlmaier,[c] S. Schmiechen,[c] C. Feldmann,[b] W. Schnick[c] and K. Müller-Buschbaum[*a]

The series of anhydrous lanthanide chlorides LnCl$_3$, Ln = Pr–Tb, and 4,4′-bipyridine (bipy) constitute isotypic MOFs of the formula $^2_\infty$[Ln$_2$Cl$_6$(bipy)$_3$]·2bipy. The europium and terbium containing compounds both exhibit luminescence of the referring trivalent lanthanide ions, giving a red luminescence for Eu^{3+} and a green luminescence for Tb^{3+} triggered by an efficient antenna effect of the 4,4′-bipyridine linkers. Mixing of different lanthanides in one MOF structure was undertaken to investigate the potential of this MOF system for colour tuning of the luminescence. Based on the gadolinium containing compound, co-doping with different amounts of europium and terbium proves successful and yields solid solutions of the formula $^2_\infty$[Gd$_{2-x-y}$Eu$_x$Tb$_y$Cl$_6$(bipy)$_3$]·2bipy (**1–8**), $0 \leq x$, $y \leq 0.5$. The series of MOFs exhibits the opportunity of tuning the emission colour in-between green and red. Depending on the atomic ratio Gd:Eu:Tb, the yellow region was covered for the first time for an oxygen/carboxylate-free MOF system. In addition to a ligand to metal energy transfer (LMET) from the lowest ligand-centered triplet state of 4,4′-bipyridine, a metal to metal energy transfer (MMET) between 4f-levels from Tb^{3+} to Eu^{3+} is as well vital for the emission colour. However, no involvement of Gd^{3+} in energy transfers is observed rendering it a suitable host lattice ion and connectivity centre for diluting the other two rare earth ions in the solid state. The materials retain their luminescence during activation of the MOFs for microporosity.

Introduction

Since the invention of metal–organic framework (MOF) chemistry including lanthanide elements, luminescence has been discussed as a potential property for this class of coordination polymers.[1–14] Two principles can be distinguished: (a) a process triggered by an organic chromophore being responsible for both the excitation and the emission process[15,16] and (b) incorporation of metal ions as luminescence centres[12–14,17–19] being mainly focussed on the use of lanthanide ions. Different from deactivation by radiation, either by a singlet–singlet transfer to the ground state (*molecular fluorescence*, S$_1$ → S$_0$) or by a

triplet–singlet transfer to S$_0$ by the spin forbidden transition T$_1$ → S$_0$ (*molecular phosphorescence*) of the organic part of a MOF, in the case of lanthanides, the emission is due to intra-configurational f–f transitions within the 4f shell.[20] As several trivalent lanthanide ions provide sufficient band gaps between their 4f states, they are useful as luminescence centres for the visible range (Sm^{3+}, Eu^{3+}, Tb^{3+}, Dy^{3+}, Tm^{3+}) and the near-infrared region (Nd^{3+}, Yb^{3+}, Er^{3+} and to a lesser extent Pr^{3+}, Sm^{3+}, Dy^{3+}, Ho^{3+}, Tm^{3+});[21] Gd^{3+} can emit in the ultraviolet region.[21] However, as the referring 4f–4f transitions are parity forbidden,[20] these transitions are usually weak in intensity. Therefore and although the photoluminescence of lanthanide ions can be an efficient process, the lanthanides suffer from weak light absorption. As the molar absorption coefficients of the trivalent lanthanides are smaller than $\varepsilon = 10$ L mol^{-1} cm^{-1}, for most transitions in the absorption spectra, only weak amounts of radiation are absorbed by direct 4f excitation. The intensity of luminescence is proportional to the luminescence quantum yield as well as to the amount of light absorbed. Consequently, limited light absorption results in weak intensity of the luminescence. This problem can be overcome by adding ligands to the system that can be utilized as potential antennas for the metal ions, the so-called antenna effect or sensitization. Regarding a MOF, its linkers may undergo a non-radiative transition from the triplet

[a]Institute for Inorganic Chemistry, Julius-Maximilians-University Würzburg, Am Hubland, 97074 Würzburg, Germany. E-mail: k.mueller-buschbaum@uni-wuerzburg.de; Fax: +49-931-3184785; Tel: +49-931-3188724

[b]Institute for Inorganic Chemistry, Karlsruhe Institute of Technology (KIT), Engesserstr. 15, 76131 Karlsruhe, Germany. E-mail: claus.feldmann@kit.edu; Fax: +49-721-6084892; Tel: +49-721-6082856

[c]Department of Chemistry, University of Munich (LMU), Butenandtstr. 5-13, 81377 München, Germany. E-mail: wolfgang.schnick@uni-muenchen.de; Fax: +49-89-218077440; Tel: +49-89-218077436

† Electronic supplementary information (ESI) available. See DOI: 10.1039/c2jm15571k

This journal is © The Royal Society of Chemistry 2012

J. Mater. Chem., 2012, **22**, 10179–10187 | 10179

state to an excited 4f state of the lanthanide ion.[22] Subsequent to this indirect excitation by energy transfer, the lanthanide ion may undergo a radiative transition to a lower 4f state by characteristic line-like photoluminescence, *e.g.* intense metal-centred luminescence can be observed for lanthanide complexes with organic ligands like salicylic aldehyde, benzoyl acetone, and dibenzoyl methane upon excitation in an absorption band of the organic ligand.[23] A much higher amount of light can be absorbed by the organic ligands than by the lanthanide ion itself because of the intense absorption bands of the organic chromophores. Though the phenomenon that the ligand in a system can be utilized for a much more efficient excitation process was discovered almost 70 years ago,[23] it was correctly evaluated much later, while today it is a prominent feature for luminescent lanthanide containing MOFs.[24] Providing a sufficient overlap of excited states of the ligands with excited 4f states of the lanthanides, a ligand to metal energy transfer (LMET) becomes available.[24] Emission is then provided by the lanthanide ions as the expected line emission of the referring lanthanide ions. Because the partially filled 4f shell is shielded from the chemical environment by the closed $5s^2$ and $5p^6$ shells, the ligands in the first and second coordination sphere hardly perturb the electronic configurations of all trivalent lanthanide ions except Ce^{3+}. This shielding is responsible for the specific properties of lanthanide luminescence including the line emission. We achieved luminescent MOFs that exhibit such processes by utilizing 4,4′-bipyridine as antenna together with trichlorides of europium and terbium accompanied by co-doping of both ions into a gadolinium MOF matrix during MOF formation. Gd^{3+} is substituted by Eu^{3+} and Tb^{3+} to give a series of solid solutions. This enables complete colour tuning within one homogeneous MOF material. Recently, we were able to show that co-doping of lanthanide luminescence centres into coordination polymers is possible for alkaline earth imidazolates for both divalent and trivalent lanthanide ions.[25] Co-doping of trivalent terbium and europium was observed quite recently for a coordination polymer statistically distributing the different lanthanide ions over the metal sites of the network[26] and in a lanthanum based carboxylate for very low doping amounts,[27] rendering colour tuning accessible and corroborating our observation.

We can now show that higher amounts of trivalent lanthanide ions enable additional energy transfer mechanisms, namely a metal to metal energy transfer (MMET) from excited 4f states of Tb^{3+} to excited 4f states of Eu^{3+} that can be further used for the colour tuning of the emission. This energy transfer from Tb^{3+} to Eu^{3+} was also observed for a mixed europium/terbium adipate framework[28] featuring the role of intercalated 4,4′-bipyridine as non-coordinated organic sensitizer moieties in the solid state of a carboxylate MOF. Further metal to metal energy transfers were *e.g.* also shown between Tb^{3+} and Yb^{3+} resulting in an IR emission at 980 nm, or between Ag^+ and Eu^{3+} combined to major increase of the intensity of the hypersensitive transition $^5D_0 \rightarrow {}^7F_2$ of Eu^{3+}.[29,30] It is evident that apart from upconversion, the energy transfer can only be observed from a higher or equal energy level of the sensitizer to an acceptor energy level. The influence of activation for microporosity of our materials on the luminescence was also investigated retaining the luminescence after evaporation of the 4,4′-bipyridine templates.

Results and discussion

### Solvent free synthesis of $^2_\infty[Gd_{2-x-y}Eu_xTb_yCl_6(bipy)_3] \cdot 2bipy$ (1–8)

For the synthesis of the series of compounds $^2_\infty[Ln_2Cl_6(bipy)_3] \cdot (bipy)_2$ with Ln = Gd and $Gd_{2-x-y}Eu_xTb_y$ (1–8) a solvent-free reaction route *via* a self-consuming organic melt synthesis was utilized.[31] Mixtures of $GdCl_3$, $EuCl_3$ and $TbCl_3$ were directly reacted with molten 4,4′-bipyridine to give the MOFs as a series of solid solutions. Thereby co-coordination of unwanted solvent molecules is avoided. Providing a suitable antenna for luminescence by the use of bipyridine as the linker of the framework, the avoidance of solvent molecules can be additionally valuable as quenching effects of the solvent are suppressed. Instead 4,4′-bipyridine is incorporated in the channels, which is known to act as a sensitizer even by radiation only.[28] Thereby molten organic ligands can act as both suitable linkers and templates for the formation of a luminescent network structure leading to two-dimensional coordination polymers or MOFs.[32] As the pure gadolinium containing MOF compound 1 constituted from $GdCl_3$ has not been known before, it was also synthesized for comparison.

For 1 anhydrous $GdCl_3$ and for 2–8 different ratios of anhydrous chlorides $LnCl_3$ with Ln = Eu, Gd, and Tb were ground with 4,4′-bipyridine and the batches were sealed in glass ampoules under vacuum. The samples were slowly heated above the melting point of the free ligand for reaction. The cooldown process is used for annealing and increases the crystallinity of the products. Powder X-ray diffraction PXRD measurements indicate phase purity and confirm high yields of the compounds.

Crystal structure of $^2_\infty[Gd_{2-x-y}Eu_xTb_yCl_6(bipy)_3] \cdot 2bipy$ (1–8)

The crystal structures of 1 and of the mixed lanthanide MOFs 2–8 are isotypic to one another and to the compounds $^2_\infty[Ln_2Cl_6(bipy)_3] \cdot 2bipy$ with the lanthanides Ln = Pr, Nd, Sm, Eu and Tb.[32] This was proven by single-crystal as well as powder X-ray diffraction. Refinement of the lattice parameters of 1 was done on the diffraction pattern on a series of reflections with the best possible resolution leading to a triclinic unit cell with no unindexed reflections.[3] Comparison of the powder patterns of the complete series 1–8 with simulated diffractograms on the basis of X-ray single-crystal data of the isotypic Eu-MOF[32] confirms the isotypic character of 1–8, the co-doped frameworks being solid solutions (see ESI†). Exemplarily for compounds 1–8, the results of the PXRD investigation on the mixed crystal 7 are shown in Fig. 1 in comparison to a simulated powder pattern of $^2_\infty[Eu_2Cl_6(bipy)_3] \cdot 2bipy$ derived from single-crystal data.

All compounds crystallize in the triclinic space group $P\bar{1}$. The trivalent Ln^{3+} ions can be located on one crystallographic site and exhibit a coordination number of 7 with a pentagonal bipyramidal configuration. The metal ions are coordinated by two terminal (η^1) and two bridging (μ^2) chloride anions as well as three additional neighbouring N atoms of 4,4′-bipyridine molecules. Thereby an edge connected pentagonal-bipyramidal SBU (secondary building unit) is formed. The single crystallographic site of Ln^{3+} is statistically occupied by the corresponding Ln^{3+} ions in 2–8 due to their similar ionic radii (Eu^{3+} = 115 pm, Gd^{3+} = 114 pm and Tb^{3+} = 112 pm at C.N. = 7).[33] The match in radii together with the similarity in oxidation state and chemical
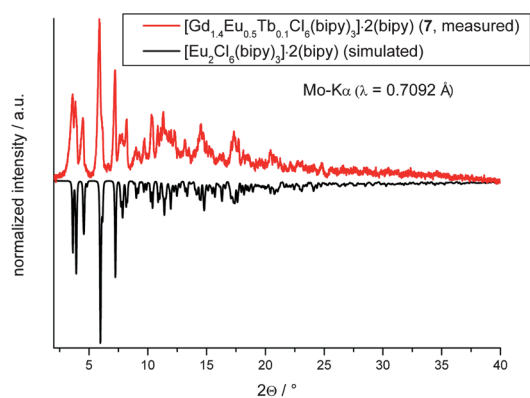
Fig. 1 Powder diffractogram of **7** (measured) compared to the powder diffractogram of the isotypic $^2_\infty$[Eu$_2$Cl$_6$(bipy)$_3$]·2bipy (calculated).

behaviour is the key to the formation of a series of mixed crystal for all ratios of the three lanthanide ions allowing much higher and variable concentrations of the luminescence centres compared to a usual co-doping of a host lattice. The interconnection of the SBUs *via* six bipy molecules leads to a 2D layer structure (Scheme 1) with *mmm* symmetry for each layer. The layers are horizontally shifted to one another along the Ln$_2$Cl$_6$-dimer longitudinal axis, creating 180° twisted trapezoid like channels with intercalated template bipy molecules. This leads to a reduction of the overall symmetry to $P\bar{1}$ (Fig. 2). As the structure and mainly interatomic angles and distances were already discussed in ref. 32, the reader is referred to it for further information.[32]

Vibrational spectroscopy

For the series of MOFs **1–8** MIR spectra were recorded. They show combined signals for the vibrations of 4,4′-bipyridine that derive from coordinated and intercalated bipy and their vibration nodes. The vibrational behaviour of the coordinated species resembles that of the known complex compounds M(bipy)Cl$_2$ with M = Zn, Cu, and Cd[34] or LnCl$_3$(bipy)$_2$·H$_2$O$_n$ with Ln = Dy,
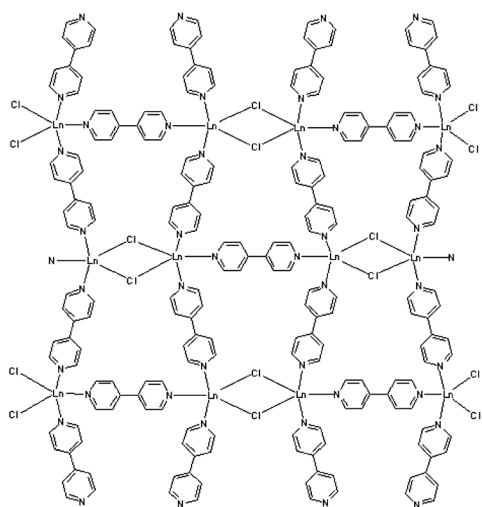
Scheme 1 Connectivity of a single layer sheet of $^2_\infty$[Ln$_2$Cl$_6$(bipy)$_3$] (**1–8**). The layers exhibit a 4,4-topology.
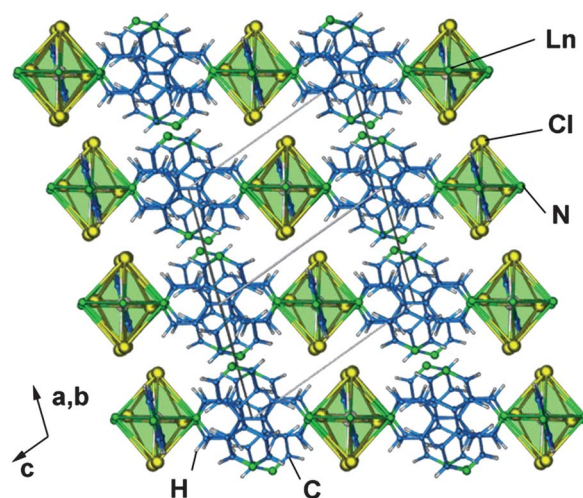
Fig. 2 Depiction of the 2D layer structure of $^2_\infty$[Ln$_2$Cl$_6$(bipy)$_3$]·2bipy. View along the longitudinal axis of the Ln$_2$Cl$_6$ dimers.

Ho, Er, Tm, and Yb,[35] and of course the series of isotypic frameworks with Pr, Nd and Sm. While the linking 4,4′-bipyridine molecules are almost planar, the aromatic rings of the intercalated 4,4′-bipyridine are rotated to a non-staggered position along its longitudinal axis. Therefore theoretical calculations for the vibration modes of polycrystalline 4,4′-bipyridine (planar molecules) are of limited use for exact identification of bands.[36]

However differences due to binding of the ligand can be identified: the centre of the v(CH) bending nodes ($\sim$3060 cm^{-1}) is raised by $\sim$35 cm^{-1} (4,4′-bipy = 3024 cm^{-1}) and v(CN) ring stretching nodes ($\sim$1601 cm^{-1}) are shifted by $\sim$5 cm^{-1} to higher frequency (4,4′-bipy = 1588 cm^{-1}). Additionally, indication for M–L bonding can be found at $\sim$1003 and $\sim$990 cm^{-1}. The single pyridine breathing mode (4,4′-bipy = 988 cm^{-1}) is split into two signals corresponding to the coordinated (higher energy) and intercalated (lower energy) 4,4′-bipy. Further signal splitting can be observed in the fingerprint area at 1218, 1038 and 606 cm^{-1}.

Photoluminescence spectroscopy

The series of solid solutions $^2_\infty$[Gd$_{2-x-y}$Eu$_x$Tb$_y$Cl$_6$(bipy)$_3$]·2bipy (**2–8**) exhibits photoluminescence (PL) properties by excitation with UV-light (max. λ_{exc} = 302 nm, see Fig. 3), whereas the pure gadolinium network compound **1** does not exhibit any luminescence emission, even the characteristic 4f–4f transition of Gd^{3+} at 311 nm is not visible. Accordingly, only europium and terbium take part in the emission. A fluent change of the visible PL emission colour between green, yellow, orange and red can be achieved by variation of the terbium and europium content. Therefore the ratio of the lanthanide ions can be used to establish complete tuning of the emission colour as an additive effect of the participating ions in this homogeneous MOF series with an oxygen-free lanthanide coordination sphere. Referring behaviour was also reported for doping low amounts of Eu^{3+} and Tb^{3+} into a lanthanum carboxylate[27] and direct mixing of the two lanthanide ions without further host lattice metal ions like Gd^{3+}.[26]

In comparison to the visual impression, the PL emission spectra (λ_{Exc} = 307 nm) of **2–8** are depicted in Fig. 4. The
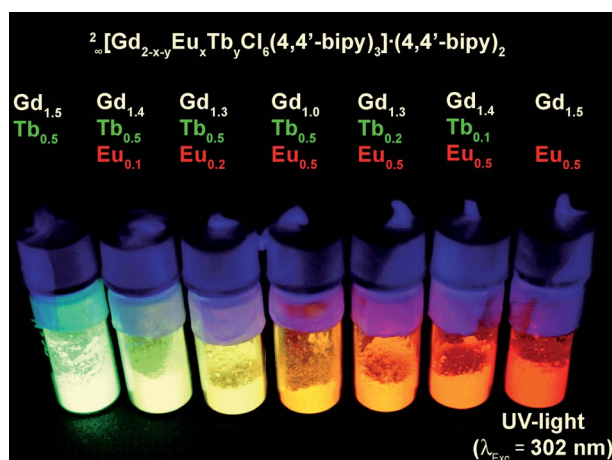
**Fig. 3** Photoluminescence of the series of solid solutions $^2_\infty[Gd_{2-x-y}Eu_xTb_yCl_6(bipy)_3]\cdot 2bipy$ under UV light ($\lambda = 302$ nm), **2–8** being arranged in increasing number from left to right.

intensity of each spectrum was normalized on its highest emission peak. The colour assignment is chosen according to the visual impression of the emission colours. The spectra show the typical intra 4f–4f transitions of Eu^{3+} and Tb^{3+} ions. The centre of the Tb^{3+} transitions $^5D_4 \rightarrow {}^7F_{6-0}$ can be detected at 488 nm, 546 nm, 588 nm, 621 nm, 652 nm, 667 nm and 680 nm. The centre of Eu^{3+} transitions $^5D_0 \rightarrow {}^7F_{0-4}$ can be observed at 579 nm, 590 nm, 616 nm, 653 nm and 702 nm.[20]

An overlap of different transitions of Eu^{3+} and Tb^{3+} between 570 and 660 nm leads to mixed transition peaks. Spectroscopically pure Tb^{3+} transitions are measured solely at 488 nm and 546 nm, and for Eu^{3+} solely at 702 nm, allowing a clean spectroscopic distinction between both lanthanides. It is remarkable that the strongest transition for Eu^{3+} is identified by $^5D_0 \rightarrow {}^7F_4$, and not by the $^7F_2$ state. This observation was previously reported for non-centrosymmetric distorted coordination spheres like the pentagonal bipyramid,[25b] and is discussed to be combined to a high polarizability of the coordinating ligands.[37] A higher ligand polarizability results in a larger overlap between the lanthanide and the ligand orbitals and thus a change in the degree of covalency between cations and ligands,[38] resulting in an
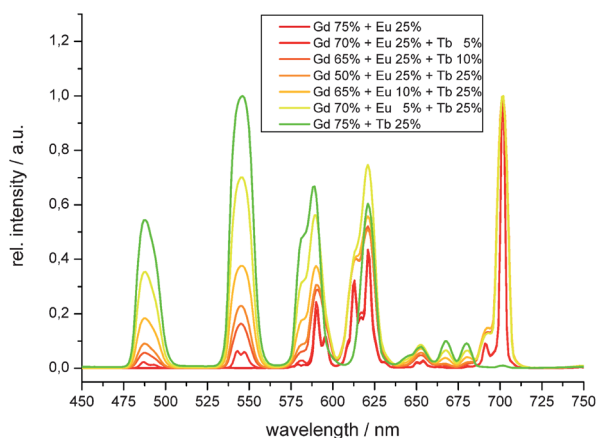
increase of the Ω_4 parameter of the Judd–Ofelt analysis.[39] The latter characterizes the intensity of the $^5D_0 \rightarrow {}^7F_4$ transition. However, there is no theoretical prediction for this sensitivity to macroscopic properties so far.[40]

The energetic positions of the transitions, their intensity distribution and the hyperfine structure of the spectra of **2** and **8** resemble the non-doped isotypic compounds that contain a concentration of 100% luminescent centres $^2_\infty[Ln_2Cl_6(bipy)_3]\cdot 2bipy$, Ln = Eu and Tb. Therefore we assume a random distribution of the emitting Eu^{3+} and Tb^{3+} ions on the single lanthanide crystallographic site of the Gd structure, leading to a statistically mixed crystal series, corroborating the discussion of a direct mixing of terbium and europium for carboxylate coordination polymers and MOFs.[26,29]

Tuning of the emission colour can be quantitatively characterized by the use of colour coordinates according to the *CIE 1931* diagram.[41] Colour coordinates for compounds **2–8** are given in Table 1 and visualized in Fig. 5.

In addition a metal-to-metal energy transfer (MMET) between Tb^{3+} and Eu^{3+} can be observed. Compounds **5–8** contain the same amount of Eu^{3+} and changing proportions of Gd^{3+} and Tb^{3+} ions. The absolute intensity of the spectroscopic pure Eu^{3+} transition $^5D_0 \rightarrow {}^7F_4$ increases with an increasing amount of Tb^{3+} while the Eu^{3+} amount remains constant (Fig. 6). Therefore we assume a direct energetic relation between the two different luminescent centres, as observed for a mixed terbium/europium adipate framework.[29]

The series of MOFs **2–8** shows an additional energy transfer: the PL excitation spectra ($\lambda_{Em} = 702$ nm, Eu^{3+}: $^5D_0 \rightarrow {}^7F_4$) of **5–8** (Fig. 6) show a large, broad excitation band in the UV area with a maximum at 307 nm. This band can be identified with the excitation of 4,4′-bipyridine $S_0 \rightarrow S_1$. Followed by a singlet–triplet transfer the ligand reaches an excited state with a lower energy. As the emission spectra recorded for this excitation maximum show lanthanide emission only and no organic fluorescence, the networks show an efficient ligand-to-metal energy transfer (LMET) from 4,4′-bipyridine to the corresponding Eu^{3+} and Tb^{3+} ions, which is called the antenna effect (see Fig. 7 for the energy transfer processes).[42]

Furthermore additional but rather weak intra 4f–4f transitions of Tb^{3+} ($^7F_6 \rightarrow {}^{2S+1}L$ at 345–395 nm, $^7F_6 \rightarrow {}^5D_4 \rightarrow$ at 488 nm) and Eu^{3+} ($^7F_0 \rightarrow {}^5D_4$ at 361 nm, $^7F_0 \rightarrow {}^5D_3$ at 393 nm and $^7F_0 \rightarrow {}^5D_2$ at 464 nm) can be observed confirming the possibility of additional direct excitation of the luminescent centres *via* their intraconfigurational 4f–4f transitions (see Fig. 8). However, direct excitation of Tb^{3+} and Eu^{3+} is weak compared to the excitation *via* the linker ligand. Gadolinium is neither present in the excitation nor in the emission parts of the PL spectra

Fig. 4 Depiction of normalized PL emission spectra of **2–8**. ($\lambda_{Exc} = 307$ nm).

Table 1 Colour coordinates of **2–8** according to *CIE 1931*

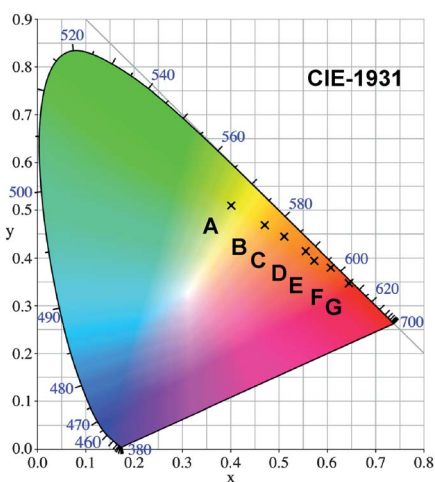|	$^2_\infty[Ln_2Cl_6(bipy)_3]\cdot bipy_2$	No.	X	Y
A	$Gd_{1.5}Tb_{0.5}$	**2**	0.401	0.510
B	$Gd_{1.4}Eu_{0.1}Tb_{0.1}$	**3**	0.470	0.468
C	$Gd_{1.3}Eu_{0.2}Tb_{0.5}$	**4**	0.510	0.445
D	$GdEu_{0.5}Tb_{0.5}$	**5**	0.555	0.414
E	$Gd_{1.3}Eu_{0.5}Tb_{0.2}$	**6**	0.572	0.394
F	$Gd_{1.4}Eu_{0.5}Tb_{0.1}$	**7**	0.607	0.380
G	$Gd_{1.5}Eu_{0.5}$	**8**	0.643	0.346

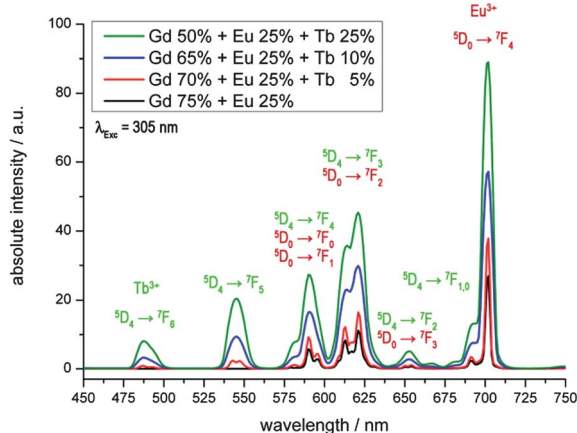**Fig. 5** Colour coordinate diagram of compounds **2–8**.

Fig. 6 PL emission spectra ($\lambda_{Exc} = 307$ nm) of **5–8** shown as absolute intensities identifying the increase of Eu emission by MMET.

indicating that it is neither directly excited nor present in the emission process (307 nm). In principle, Gd^{3+} can be involved in a LMET as its excited 4f state matches with the excited S_1 state of bipy. Due to the short lifetime of the excited singlet states of the aromatic ligand, this probability is low combined to a possible energy backtransfer process to the ligand. Different from Eu^{3+} and Tb^{3+} that can populate excited ^5D_x states close in energy on a reduced energy level that are reached by non-radiative relaxation[20] reducing the amount of energy backtransfer significantly, Gd^{3+} only provides a large band gap to the ground state (see Fig. 9). An energy transfer from the T_1 state of the ligand to Gd^{3+} is not possible as gadolinium does not provide energy levels in the referring region. The impact of Gd^{3+} is its utilization as a matrix to dilute the two other lanthanide ions within a majority of gadolinium connectivity centres and thereby reducing the amount of luminescence centres and thus a potential quenching by concentration.

Activation and adsorption experiments

For the series of MOFs **1–8** activation under evaporation of the template 4,4′-bipyridine molecules was investigated. Therefore
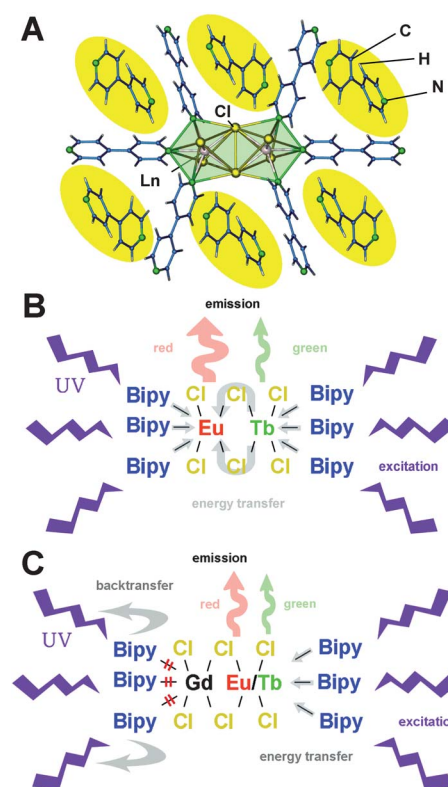

Fig. 7 Schematic depiction of the energy transfer processes between metal ions and ligands in **2–8** in comparison with the crystal structure.

the MOFs were outgassed at a vacuum of 10^{-2} mbar for 72 h at varying temperatures ranging from 100 to 315 °C. Nitrogen adsorption–desorption isotherms were recorded at −196 °C in the relative pressure range 10^{-6} to 1 atm. The results were compared to the non-activated framework **1**. While the non-activated MOF is simply dense due to the templates, increasing amounts of N_2 can be incorporated (up to 172 cm^3 g^{-1} for an activation of **1** at 315 °C, Fig. 10) with regard to the activation temperature. This corresponds to a surface area of $s_{BET} = 660$ m^2 g^{-1}. The isotherms acquired by activation at 300 °C and 315 °C indicate that in addition to the microporosity of the framework's

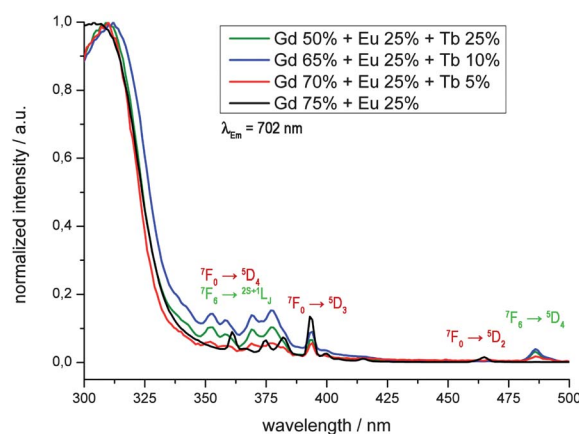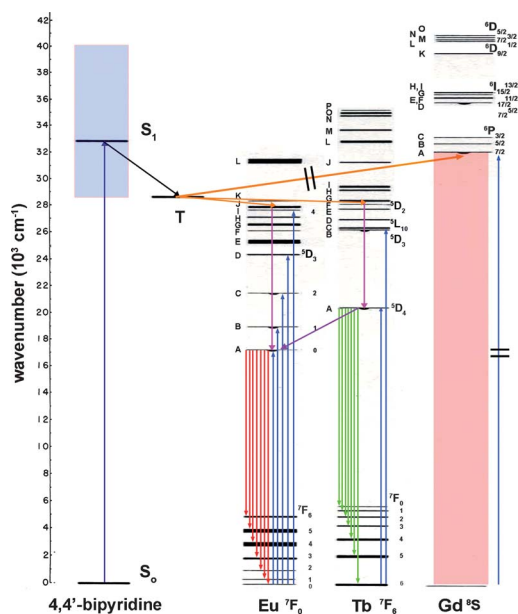**Fig. 8** PL excitation spectra ($\lambda_{Em} = 702$ nm) of **5–8** shown as absolute intensities.

Fig. 9 Excitation and emission processes between metal ions and ligands in $_{\infty}^{2}$[Gd$_{2-x-y}$Eu$_x$Tb$_y$Cl$_6$(bipy)$_3$]·2bipy (**2–8**).

crystal structure a low mesoporosity is observed, which is also present in the pore size distribution ranging from 0.6 to 1.8 nm for N_2 adsorption. The activated luminescent MOFs **2–8** retain their luminescence upon activation, indicating that the framework structure is also maintained. Higher activation temperatures under vacuum are not suitable as the MOFs then release framework constituting bipy molecules. In order to further investigate and corroborate these findings, X-ray powder diffraction and simultaneous DTA/TG investigations were carried out to monitor the activation process. Thermal analyses show that the non-coordinating molecules are released first prior to release of the coordinating bipy molecules (see ESI†). XRPD including temperature dependent investigations matches this observation as the diffractograms exhibit a significant change upon release of coordinating 4,4′-bipyridine molecules as this also implies a constitutional change of the network (see ESI†). Accordingly, activation temperatures have to be kept below.
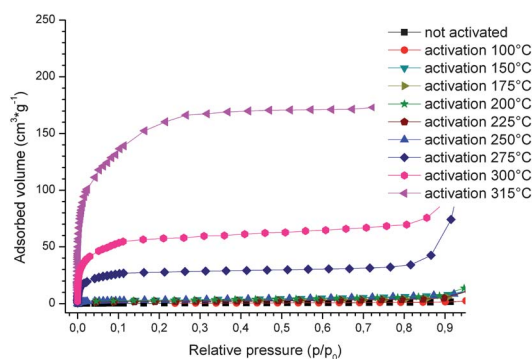
Fig. 10 N_2 adsorption isotherms at −196 °C for $_{\infty}^{2}$[Gd$_2$Cl$_6$(bipy)$_3$]·2bipy (**1**) in cm^3 g^{-1} uptake depending on the variation of the activation temperature of the MOF.

Conclusions

The MOF system $_{\infty}^{2}$[Ln$_2$Cl$_6$(bipy)$_3$]·2bipy can be successfully used for an efficient tuning of the emission colour. During MOF formation different ratios of Eu^{3+} and Tb^{3+} can be implemented into the MOF by mixing their trichlorides with GdCl$_3$ under solvent free melt conditions of 4,4′-bipyridine, as the three trivalent lanthanides form a series of mixed crystal MOFs. Depending on the ratio of the three lanthanides networks of the formula $_{\infty}^{2}$[Gd$_{2-x-y}$Eu$_x$Tb$_y$Cl$_6$(bipy)$_3$]·2bipy, $0.1 \leq x$, $y \leq 0.5$, are formed. 4,4′-Bipyridine functions as an antenna providing a ligand to metal T$_1$ → 4f energy transfer (LMET) to both Eu^{3+} and Tb^{3+}. The combination of europium and terbium further renders an additional partial metal to metal energy transfer (MMET) available from Tb^{3+} to Eu^{3+} excited 4f states. This leads to an increase of the emission in the red region due to the increasing intensity of the Eu^{3+} emission. In the combinatorial observation emission of both europium and terbium is visible depending on their ratio and emission intensities. As the strengthening of the red region balances our eye being more sensitive in the green region, a perfect series of luminescence tuned hybrid material can be formed that covers the complete visible spectrum in-between green and red emission including yellow and orange. As Gd^{3+} is not involved in the radiative processes it can be utilized as a matrix to dilute the two other lanthanide ions within a majority of gadolinium connectivity centers providing a series of isotypic solid solutions of all three ions. The materials become even more interesting as luminescence is retained during activation of the MOFs for microporous materials.

Experimental

All manipulations were carried out under inert gas atmosphere using a glovebox (MBraun Labmaster, Ar atmosphere), Schlenk technique and DURAN™ ampoules as well as vacuum line techniques. Heating furnaces with Al$_2$O$_3$ tubes together with Eurotherm 2416 control elements were used for the purpose of heating the ampoule experiments. Trichlorides LnCl$_3$, Ln = Gd, Eu and Tb, were prepared by the published ammonium halide route[43] using the oxides Ln$_2$O$_3$ (ChemPur, 99.9%), HCl solution (10 mol l^{-1}, reagent grade) and ammonium chloride (Fluka, 99.5%), and purified by decomposition of the trivalent ammonium chlorides under vacuum and subsequent sublimation of the products. 4,4′-Bipyridine (Alfa Aesar, 98%) was used as purchased. All products are air and moisture sensitive. For microanalysis, PXRD, vibrational spectroscopy as well as photoluminescence spectroscopy the microcrystalline materials were purified by evaporating excess 4,4′-bipyridine.

General consideration on the synthesis of $_{\infty}^{2}$[Gd$_{2-x-y}$Eu$_x$Tb$_y$Cl$_6$(bipy)$_3$]·2bipy (1–8)

For the synthesis of **1–8** the reagents were mixed by grinding and sealed in evacuated Duran glass ampoules. The reaction mixtures were heated to 90 °C in 4 h and to 120 °C in 30 h. This temperature was maintained for 48 h. The reaction mixture was then cooled to 95 °C in 250 h and to room temperature within another 12 h. The products obtained were purified by

10184 | *J. Mater. Chem.*, 2012, **22**, 10179–10187

This journal is © The Royal Society of Chemistry 2012

evaporation of excess 4,4′-bipyridine in a temperature gradient 120 °C → RT. The reactions led to microcrystalline, colourless powders.

Synthesis of $^2_\infty$[Gd$_2$Cl$_6$(bipy)$_3$]·2bipy (1)

GdCl$_3$ (0.5 mmol = 132 mg) and 4,4′-bipyridine (C$_{10}$H$_8$N$_2$, 1.5 mmol = 234 mg) were ground and transferred into an ampoule. The corresponding experimental procedure including the heating program is described above. Yield: 272 mg = 83%. Anal. Calcd for C$_{50}$Cl$_6$H$_{40}$N$_{10}$Gd$_2$ (M_r = 1308.16 g mol^{-1}): C, 45.90; N, 10.70; H, 3.08. Found: C, 45.37; N, 10.64; H, 2.97%. MIR (KBr): (3055 m, 1602 vs, 1533 s, 1485 m, 1414 m, 1318 w, 1225 m, 1073 wsh, 1056 m, 1043 m, 1002 m, 989 m, 801 vs, 729 m, 676 w, 625 s, 608 s, 570 m, 518 s) cm^{-1}.

Synthesis of $^2_\infty$[Gd$_{1.5}$Tb$_{0.5}$Cl$_6$(bipy)$_3$]·2bipy (2)

GdCl$_3$ (0.375 mmol = 99 mg), TbCl$_3$ (0.125 mmol = 33 mg) and 4,4′-bipyridine (C$_{10}$H$_8$N$_2$, 1.5 mmol = 234 mg) were ground in a mortar and transferred to an ampoule. The corresponding experimental procedure is described above. Yield: 278 mg = 85%. Anal. Calcd for C$_{50}$Cl$_6$H$_{40}$N$_{10}$Gd$_{1.5}$Tb$_{0.5}$ (M_r = 1308.99 g mol^{-1}): C, 45.89; N, 10.70; H, 3.08. Found: C, 45.09; N, 10.65; H, 3.07%. MIR (KBr): (3059 m, 1602 vs, 1531 s, 1487 m, 1413 m, 1319 w, 1216 m, 1070 wsh, 1060 m, 1043 m, 1003 m, 991 m, 800 vs, 731 s, 675 w, 625 s, 608 m, 571 m, 520 s) cm^{-1}.

Synthesis of $^2_\infty$[Gd$_{1.4}$Eu$_{0.1}$Tb$_{0.5}$Cl$_6$(bipy)$_3$]·2bipy (3)

GdCl$_3$ (0.350 mmol = 92 mg), EuCl$_3$ (0.025 mmol = 7 mg), TbCl$_3$ (0.125 mmol = 33 mg) and 4,4′-bipyridine (C$_{10}$H$_8$N$_2$, 1.5 mmol = 234 mg) were ground in a mortar and transferred to an ampoule. The corresponding experimental procedure is described above. Yield: 262 mg = 80%. Anal. Calcd for C$_{50}$Cl$_6$H$_{40}$N$_{10}$Gd$_{1.4}$Eu$_{0.1}$Tb$_{0.5}$ (M_r = 1308.46 g mol^{-1}): C, 45.90; N, 10.70; H, 3.08. Found: C, 44.82; N, 10.66; H, 3.04%. MIR (KBr): (3059 m, 1601 vs, 1531 s, 1488 m, 1413 m, 1319 w, 1222 m, 1070 wsh, 1060 m, 1043 m, 1003 m, 990 m, 801 vs, 731 m, 674 w, 624 s, 610 m, 572 m, 519 s) cm^{-1}.

Synthesis of $^2_\infty$[Gd$_{1.3}$Eu$_{0.2}$Tb$_{0.5}$Cl$_6$(bipy)$_3$]·2bipy (4)

GdCl$_3$ (0.325 mmol = 86 mg), EuCl$_3$ (0.050 mmol = 13 mg), TbCl$_3$ (0.125 mmol = 33 mg) and 4,4′-bipyridine (C$_{10}$H$_8$N$_2$, 1.5 mmol = 234 mg) were ground in a mortar and transferred to an ampoule. The corresponding experimental procedure is described above. Yield: 281 mg = 86%. Anal. Calcd for C$_{50}$Cl$_6$H$_{40}$N$_{10}$Gd$_{1.3}$Eu$_{0.2}$Tb$_{0.5}$ (M_r = 1307.94 g mol^{-1}): C, 45.92; N, 10.71; H, 3.08. Found: C, 44.92; N, 10.69; H, 3.06%. MIR (KBr): (3059 m, 1602 vs, 1531 s, 1488 m, 1413 m, 1319 w, 1220 m, 1070 wsh, 1060 m, 1043 m, 1003 s, 991 m, 800 vs, 730 m, 676 w, 625 s, 608 m, 570 m, 518 s) cm^{-1}.

Synthesis of $^2_\infty$[GdEu$_{0.5}$Tb$_{0.5}$Cl$_6$(bipy)$_3$]·2bipy (5)

GdCl$_3$ (0.250 mmol = 66 mg), EuCl$_3$ (0.125 mmol = 32 mg), TbCl$_3$ (0.125 mmol = 33 mg) and 4,4′-bipyridine (C$_{10}$H$_8$N$_2$, 1.5 mmol = 234 mg) were ground in a mortar and transferred to an ampoule. The corresponding experimental procedure is

described above. Yield: 254 mg = 78%. Anal. Calcd for C$_{50}$Cl$_6$H$_{40}$N$_{10}$GdEu$_{0.5}$Tb$_{0.5}$ (M_r = 1306.35 g mol^{-1}): C, 45.97; N, 10.72; H, 3.09. Found: C, 44.95; N, 10.55; H, 3.07%. MIR (KBr): (3059 m, 1601 vs, 1530 s, 1487 m, 1413 m, 1318 w, 1217 m, 1072 wsh, 1060 m, 1040 m, 1003 s, 990 m, 800 vs, 730 s, 676 w, 623 s, 609 m, 571 m, 518 s) cm^{-1}.

Synthesis of $^2_\infty$[Gd$_{1.3}$Eu$_{0.5}$Tb$_{0.2}$Cl$_6$(bipy)$_3$]·2bipy (6)

GdCl$_3$ (0.325 mmol = 86 mg), EuCl$_3$ (0.125 mmol = 32 mg), TbCl$_3$ (0.050 mmol = 13 mg) and 4,4′-bipyridine (C$_{10}$H$_8$N$_2$, 1.5 mmol = 234 mg) were ground in a mortar and transferred to an ampoule. The corresponding experimental procedure is described above. Yield: 277 mg = 85%. Anal. Calcd for C$_{50}$Cl$_6$H$_{40}$N$_{10}$Gd$_{1.3}$Eu$_{0.5}$Tb$_{0.2}$ (M_r = 1305.85 g mol^{-1}): C, 45.99; N, 10.73; H, 3.09. Found: C, 44.29; N, 10.48; H, 3.04%. MIR (KBr): (3060 m, 1601 vs, 1531 s, 1488 m, 1413 m, 1318 w, 1218 m, 1075 wsh, 1060 m, 1040 m, 1004 s, 990 m, 800 vs, 731 s, 676 w, 609 m, 572 m, 520 s) cm^{-1}.

Synthesis of $^2_\infty$[Gd$_{1.4}$Eu$_{0.5}$Tb$_{0.1}$Cl$_6$(bipy)$_3$]·2bipy (7)

GdCl$_3$ (0.350 mmol = 92 mg), EuCl$_3$ (0.125 mmol = 32 mg), TbCl$_3$ (0.025 mmol = 7 mg) and 4,4′-bipyridine (C$_{10}$H$_8$N$_2$, 1.5 mmol = 234 mg) were ground in a mortar and transferred into an ampoule. The corresponding experimental procedure is described above. Yield: 261 mg = 80%. Anal. Calcd for C$_{50}$Cl$_6$H$_{40}$N$_{10}$Gd$_{1.4}$Eu$_{0.5}$Tb$_{0.1}$ (M_r = 1305.68 g mol^{-1}): C, 46.00; N, 10.73; H, 3.09. Found: C, 44.57; N, 10.58; H, 3.03%. MIR (KBr): (3061 m, 1598 vs, 1531 s, 1489 m, 1411 m, 1316 w, 1218 m, 1073 wsh, 1065 m, 1043 m, 1002 m, 986 w, 800 vs, 731 s, 675 w, 625 s, 610 m, 573 m, 520 s) cm^{-1}.

Synthesis of $^2_\infty$[Gd$_{1.5}$Eu$_{0.5}$Cl$_6$(bipy)$_3$]·2bipy (8)

GdCl$_3$ (0.375 mmol = 99 mg), EuCl$_3$ (0.125 mmol = 32 mg) and 4,4′-bipyridine (C$_{10}$H$_8$N$_2$, 1.5 mmol = 234 mg) were ground in a mortar and transferred to an ampoule. The corresponding heating program is mentioned above. Yield: 272 mg = 83%. Anal. Calcd for C$_{50}$Cl$_6$H$_{40}$N$_{10}$Gd$_{1.5}$Eu$_{0.5}$ (M_r = 1305.51 g mol^{-1}): C, 46.00; N, 10.73; H, 3.09. Found: C, 44.68; N, 10.64; H, 3.03%. MIR (KBr): (3060 m, 1602 vs, 1531 s, 1487 m, 1413 s, 1318 w, 1225 m, 1072 wsh, 1060 m, 1043 wsh, 1003 m, 989 m, 814 msh, 800 vs, 729 m, 675 w, 626 s, 607 m, 570 m, 518 s) cm^{-1}.

X-Ray diffraction

The solid solutions $^2_\infty$[Gd$_{2-x-y}$Eu$_x$Tb$_y$Cl$_6$(bipy)$_3$]·(bipy)$_2$ (1–8) were investigated by X-ray powder diffraction and compared to each other as well as to the results of 1 (see ESI†).[32] The investigations confirmed the isotypic structural relation to $^2_\infty$[Ln$_2$Cl$_6$(bipy)$_3$]·2bipy. X-Ray powder diffraction data were collected in the Debye–Scherrer geometry on a STOE Stadi P powder diffractometer with Ge(111)-monochromatized Mo-Kα_1 (λ = 0.70926 Å) and Cu-Kα_1 (λ = 1.54056 Å) radiation. The powder pattern of $^2_\infty$[Gd$_2$Cl$_6$(bipy)$_3$]·2bipy (1) was also compared to a simulated pattern of the isotypic phase $^2_\infty$[Eu$_2$Cl$_6$(bipy)$_3$]·2bipy based on single-crystal X-ray data.[32,44] Furthermore temperature dependent XRPD was carried out on 1 to identify the range of possible activation temperatures of the

This journal is © The Royal Society of Chemistry 2012

J. Mater. Chem., 2012, **22**, 10179–10187 | 10185

MOF (see ESI†). Indexing and refinement of the lattice parameters of **1** were done on a series of reflections with the best possible resolution leading to a triclinic unit cell without unindexed lines.[45] 22 characteristic reflections with an average $\delta(2\Theta)$ of 0.08° were used for the refinement (T = 293(2) K, a = 1091(2) pm, b = 1113(1) pm, c = 1196(2) pm, α = 101.8(2)°, β = 103.9(2)°, γ = 99.2(2)°, and V = 1346(3) 10⁶ pm³).[45]

Photoluminescence and vibrational spectroscopy

Excitation and emission spectra were recorded with a Horiba Jobin Yvon Fluorolog 3 photoluminescence spectrometer equipped with a 450 W Xe lamp, an integration sphere, Czerny–Turner double grating (1200 grooves per mm) excitation and emission monochromators and an FL-1073 PMT detector. Excitation spectra were recorded from 250 to 600 nm and corrected for the spectral distribution of the lamp intensity using a photodiode reference detector. Emission spectra were recorded from 300 to 750 nm and corrected for the spherical response of the monochromators and the detector using typical correction spectra provided by the manufacturer. Additionally, the 1st and 2nd harmonic oscillations of the excitation source were blocked by edge filters (400 nm).

FTIR spectra were recorded using a Bruker FTIR-IS66V-S and a Thermo Nicolet FTIR-380 spectrometer. Samples were measured in dried KBr pellets under inert conditions.

Gas adsorption properties

Volumetric uptake and specific surface areas were determined by nitrogen adsorption–desorption isotherms at −196 °C (N₂ 99.999%) obtained on a Quantachrome Autosorb 1C apparatus. Prior to the adsorption measurements, the samples were outgassed at a vacuum of 10⁻² mbar for 72 h at varying temperatures ranging from 100 °C to 315 °C. The results were compared to the non-activated framework **1**.

Thermal analysis

For thermal analysis the products were purified by evaporation of excess 4,4′-bipyridine at 110 °C under vacuum. The products were studied using a simultaneous DTA/TG (NETZSCH STA-409) with a heating rate of 10 °C min⁻¹ from 20 °C to 1000 °C. All treatments were carried out in a constant Ar-flow of 50 ml min⁻¹.

Acknowledgements

Notes and references

1 (a) B. F. Hoskins and R. Robson, *J. Am. Chem. Soc.*, 1989, **111**, 5962; (b) B. F. Abrahams, B. F. Hoskins, D. M. Michail and R. Robson, *Nature*, 1994, **369**, 727; (c) O. M. Yaghi, H. Li, C. Davis, T. Richardson and T. L. Groy, *Acc. Chem. Res.*, 1998, **31**, 474; (d) H. Le, M. Eddaoudi, M. O'Keefe and O. M. Yaghi, *Nature*, 1999, **402**, 276; (e) J. R. Long and O. M. Yaghi, *Chem. Soc. Rev.*, 2009, **38**, 1213.

2 (a) G. Ferey, *Chem. Mater.*, 2001, **13**, 3084; (b) C. Serre and G. Ferey, *J. Mater. Chem.*, 2002, **12**, 3053; (c) G. Ferey, *Chem. Soc. Rev.*, 2008, **37**, 191; (d) G. Ferey, *Dalton Trans.*, 2009, 4400.

3 (a) S. Kitagawa, R. Kitauro and S.-i. Noro, *Angew. Chem.*, 2004, **116**, 2388; (b) S. Kitagawa and K. Uemura, *Chem. Soc. Rev.*, 2005, **34**, 109; (c) J.-P. Zhang and S. Kitagawa, *J. Am. Chem. Soc.*, 2008, **130**, 907.

4 (a) H. Furukawa, N. Ko, Y. B. Go, N. Aratani, S. B. Choi, E. Choi, A. O. Yazaydin, R. Q. Snurr, M. O'Keeffe, J. Kim and O. M. Yaghi, *Science*, 2010, **239**, 424; (b) U. Müller, M. Schubert, F. Teich, H. Puetter, K. Schierle-Arndt and J. Pastre, *J. Mater. Chem.*, 2006, **16**, 626; (c) N. Ramsahye, G. Maurin, S. Bourrelly, P. L. Llewellyn, T. Devic, C. Serre, T. Loiseau and G. Ferey, *Adsorption*, 2007, **13**, 461; (d) T. Loiseau, C. Serre, C. Hugeunard, G. Fink, G. Taulelle, M. Henry, T. Bataille and G. Ferey, *Chem.–Eur. J.*, 2004, **10**, 1373; (e) H.-L. Jiang and Q. Xu, *Chem. Commun.*, 2011, **47**, 3351.

5 (a) S. Hermes, F. Schroeder, R. Chelmowski, C. Woell and R. A. Fischer, *J. Am. Chem. Soc.*, 2005, **127**, 13744; (b) J.-P. Zhang and X.-M. Chen, *Chem. Commun.*, 2006, 1689; (c) S. Kaskel, *Handbook of Pours Solids*, 2002, vol. 2, p. 1190.

6 (a) M. Eddaoudi, D. B. Moler, H. L. Li, B. L. Chen, T. M. Reineke, M. O'Keeffe and O. M. Yaghi, *Acc. Chem. Res.*, 2001, **34**, 319; (b) C. Serre, F. Millange, C. Thouvenot, N. Gardant, F. Pelle and G. Ferey, *J. Mater. Chem.*, 2004, **14**, 1540.

7 (a) C. Janiak and J. K. Vieth, *New J. Chem.*, 2010, **34**, 2366; (b) S. Kaskel, S. Schüth and M. Stöcker, *Microporous Mesoporous Mater.*, 2004, **16**, 2869.

8 (a) A. K. Cheetham, C. N. R. Rao and R. K. Feller, *Chem. Commun.*, 2006, 4780; (b) C. Daiguebonne, N. Kerbellec, K. Bernot, Y. Gerault, A. Deluzet and O. Guillou, *Inorg. Chem.*, 2006, **45**, 5399.

9 X. Guo, G. Zhu, F. Sun, Z. Li, X. Zhao, X. Li, H. Wang and S. Qiu, *Inorg. Chem.*, 2006, **45**, 2581.

10 L. Pan, N. Zheng, Y. Wu, S. Han, R. Yang, X. Huang and J. Li, *Inorg. Chem.*, 2001, **40**, 828.

11 X. P. Yang, R. A. Jones, J. H. Rivers and R. P. J. Lai, *Dalton Trans.*, 2007, 3936.

12 (a) A. I. Voloshin, N. M. Shavaleev and V. P. Kazakov, *J. Lumin.*, 2001, **93**, 191; (b) Y. Zhang, H. Shi, Y. Ke and Y. Cao, *J. Lumin.*, 2007, **124**, 51; (c) C. A. Bauer, T. V. Timofeeva, T. B. Settersten, B. D. Patterson, V. H. Liu, B. A. Simmons and M. D. Allendorf, *J. Am. Chem. Soc.*, 2007, **129**, 7136.

13 (a) A. Lan, K. Li, H. Wu, D. H. Olson, T. J. Emge, W. Ki, M. Hong and J. Li, *Angew. Chem.*, 2009, **121**, 2370; (b) Y.-Q. Huang, B. Ding, H.-B. Song, B. Zhao, P. Ren, P. Cheng and H.-G. Wang, *Chem. Commun.*, 2006, 4906.

14 (a) B. Chen, L. Wang, Y. Xiao, F. R. Fronczek, M. Xue, Y. Cui and G. Qian, *Angew. Chem.*, 2009, **121**, 508; (b) *Angew. Chem., Int. Ed.*, 2009, **48**, 500; (c) Z. Chen, B. Zhao, Y. Zhang, W. Shi and P. Cheng, *Cryst. Growth Des.*, 2008, **8**, 2291; (d) F. Gándara, A. de Andrés, B. Gómez-Lor, E. Gutiérrez-Puebla, M. Iglesias, M. A. Monge, D. M. Proserpio and N. Snejko, *Cryst. Growth Des.*, 2008, **8**, 378.

15 (a) A. Eremenkoa, N. Smirnovaa, O. Rusinaa, O. Linnika, T. B. Eremenkob, L. Spanhelc and K. Rechthalerd, *J. Mol. Struct.*, 2000, **553**, 1; (b) C. F. Ravilious, R. T. Farrara and S. H. Liebson, *J. Opt. Soc. Am.*, 1954, **44**, 238.

16 (a) H. A. Habib, J. Sanchiz and C. Janiak, *Dalton Trans.*, 2008, 1734; (b) M.-S. Wang, S.-P. Guo, Y. Li, L.-Z. Cai, J.-P. Zou, G. Xu, W.-W. Zhou, F.-K. Zheng and G.-C. Guo, *J. Am. Chem. Soc.*, 2009, **131**, 13572; (c) B. Liu, M. Ma, D. Zacher, A. Betard, K. Yusenko, N. Metzler-Nolte, C. Wöll and R. A. Fischer, *J. Am. Chem. Soc.*, 2011, **133**, 1734.

17 (a) S. Raphael, M. L. P. Reddy, A. H. Cowley and M. Findlater, *Eur. J. Inorg. Chem.*, 2008, **28**, 4387; (b) H.-M. Xiong, D. G. Shchukin, H. Möhwald, Y. Xu and Y.-Y. Xia, *Angew. Chem., Int. Ed.*, 2009, **48**, 2727; (c) K. Müller-Buschbaum, S. G. Torres, P. Larsen and C. Wickleder, *Chem. Mater.*, 2007, **19**, 655.

18 (a) J. Rocha, L. D. Carlos, F. A. Almeida Paz and D. Ananias, *Chem. Soc. Rev.*, 2011, **40**, 926; (b) B. Chen, L. Wang, F. Zapata, G. Qian and E. B. Lobkovsky, *J. Am. Chem. Soc.*, 2008, **130**, 6718.

19 (a) H. Guo, Y. Zhu, S. Qiu, J. A. Lercher and H. Zhang, *Adv. Mater.*, 2010, **22**, 4190; (b) L. Yang, Y. Zhao, Y. Su and J. Wu, *Spectrochim. Acta, Part A*, 2002, **58**, 2803.

20 (a) G. Blasse and B. C. Grabmaier, *Luminescent Materials*, Springer Verlag, Berlin, 1994; (b) G. H. Dieke, *Spectra and Energy Levels of Rare Earth Ions in Crystals*, Wiley Interscience, New York, 1968.

21 (a) K. Binnemans, *Chem. Rev.*, 2009, **109**, 4283; (b) S. V. Eliseeva and J.-C. G. Bünzli, *Chem. Soc. Rev.*, 2010, **39**, 189; (c) J.-C. G. Bünzli, *Chem. Rev.*, 2010, **110**, 2729.

22 (a) G. A. Crosby, R. E. Whan and R. M. Alire, *J. Chem. Phys.*, 1961, **34**, 743; (b) R. E. Whan and G. A. Crosby, *J. Mol. Spectrosc.*, 1962, **8**, 315; (c) G. A. Crosby, R. E. Whan and J. J. Freeman, *J. Phys. Chem.*, 1962, **66**, 2493.

23 S. I. J. Weissman, *Chem. Phys.*, 1942, **10**, 214.

24 (a) N. Sabbatini, M. Guardigli, L. Manet, R. Ungaro, A. Casnati, R. Ziessel, G. Ulrich, Z. Asfari and J.-M. Lehn, *Pure Appl. Chem.*, 1995, **67**, 135; (b) H. J. Batista, A. V. M. de Andrade, R. L. Longo, A. M. Simas, G. F. de Sa, N. K. Ito and L. C. Thompson, *Inorg. Chem.*, 1998, **37**, 3542.

25 (a) A. Zurawski, M. Mai, D. Baumann, C. Feldmann and K. Müller-Buschbaum, *Chem. Commun.*, 2011, 496; (b) A. Zurawski, J.-C. Rybak, L. Meyer, P. R. Matthes, V. Stepanenko, F. Würthner and K. Müller-Buschbaum, *Dalton Trans.*, DOI: 10.1039/c2dt12047j.

26 N. Kerbellec, D. Kustaryono, V. Haquin, M. Etienne, C. Daiguebonne and O. Guillou, *Inorg. Chem.*, 2009, **48**, 2837.

27 K. Liu, Y. Zheng, G. Jia, M. Yang, Y. Song, N. Guo and H. You, *J. Solid State Chem.*, 2010, **183**, 2309.

28 D. T. de Lill, A. de Bettencourt-Dias and C. L. Cahill, *Inorg. Chem.*, 2007, **46**, 3960.

29 S. Faulkner and S. J. A. Pope, *J. Am. Chem. Soc.*, 2003, **125**, 10526.

30 W. Liu, T. Jiao, Y. Li, Q. Liu, M. Tan, H. Wang and L. Wang, *J. Am. Chem. Soc.*, 2004, **126**, 2280.

31 (a) K. Müller-Buschbaum, *Z. Anorg. Allg. Chem.*, 2005, **631**, 811; (b) K. Müller-Buschbaum, Y. Mokaddem, F. Schappacher and R. Pöttgen, *Angew. Chem., Int. Ed.*, 2007, **46**, 4385; (c) K. Müller-Buschbaum and Y. Mokaddem, *Chem. Commun.*, 2006, 2060; (d) C. J. Höller and K. Müller-Buschbaum, *Inorg. Chem.*, 2008, **47**, 10141; (e) C. J. Höller and K. Müller-Buschbaum, *Eur. J. Inorg. Chem.*, 2010, 454; (f) K. Müller-Buschbaum and Y. Mokaddem, *Z. Anorg. Allg. Chem.*, 2008, **634**, 2360.

32 C. J. Höller, M. Mai, C. Feldmann and K. Müller-Buschbaum, *Dalton Trans.*, 2010, **39**, 461.

33 R. D. Shannon, *Acta Crystallogr., Sect. A: Cryst. Phys., Diffr., Theor. Gen. Crystallogr.*, 1976, **32**, 751.

34 S. Bayari, A. Topacli and B. Salih, *J. Mol. Struct.*, 1999, **482–483**, 165.

35 (a) D. Czakis-Sulikowska and J. Radwanska-Doczekalska, *J. Inorg. Nucl. Chem.*, 1979, **41**, 129; (b) D. Czakis-Sulikowska and J. Radwanska-Doczekalska, *Rocz. Chem.*, 1975, **49**, 197; (c) D. Czakis-Sulikowska and J. Radwanska-Doczekalska, *Rocz. Chem.*, 1976, **50**, 2181.

36 A. Topacli and S. Akyüz, *Spectrochim. Acta, Part A*, 1994, **51**, 633.

37 H. Liang and F. Xie, *Spectrochim. Acta, Part A*, 2010, **77**, 348.

38 H. F. Brito, O. L. Malta, L. R. Souza, J. F. S. Menezes and C. A. A. Carvalho, *J. Non-Cryst. Solids*, 1999, **247**, 129.

39 H. Ebendorff-Heidepriem and D. Ehrt, *J. Non-Cryst. Solids*, 1999, **248**, 247.

40 S. S. Braga, R. A. Saferreira, I. S. Goncalves, M. Pillinger, J. Rocha, J. J. C. Teixeira-Dias and L. D. Carlos, *J. Phys. Chem. C*, 2002, **106**, 11430.

41 *Phosphor Handbook*, ed. S. Shionoya and W. M. Yen, CRC Press, Boca Raton, Boston, London, New York, Washington DC, 1999.

42 Y. Kuroda, K. Sugou and K. Sasaki, *J. Am. Chem. Soc.*, 2000, **122**, 7833.

43 G. Meyer, *Inorg. Synth.*, 1989, **25**, 146.

44 (a) G. M. Sheldrick, *SHELXS-97, Program for the resolution of Crystal Structures*, Göttingen, 1997; (b) G. M. Sheldrick, *SHELXL-97, Program for the refinement of Crystal Structures*, Göttingen, 1997.

45 (a) A. A. Coelho, *TOPAS-Academic V4.1, Program for indexing, structure resolution and Rietveld refinement on powder data*, 2007; (b) *Stoe Winxpow v.2.12, Program Package for the Operation of Powder Diffractometers and Analysis of Powder Diffractograms*, STOE, Darmstadt, 2005.

This journal is © The Royal Society of Chemistry 2012

J. Mater. Chem., 2012, **22**, 10179–10187 | 10187